Model and characterization of persistence in HgCdTe SWIR detectors for astronomy application

T Le Goff, T Pichon, N Baier, O Gravrand, O Boulade

Journal of Electronic Materials (2022) 51:5586–5593
https://doi.org/10.1007/s11664-022-09854-7

ORIGINAL RESEARCH ARTICLE

Model and Characterization of Persistence in HgCdTe SWIR Detectors for Astronomy Application

T. Le Goff[1] · T. Pichon[2] · N. Baier[1] · O. Gravrand[1] · O. Boulade[2]

Received: 20 April 2022 / Accepted: 26 July 2022 / Published online: 9 August 2022

Abstract

Persistence is the remnant signal that plagues HgCdTe infrared detectors used for astronomy applications after a bright illumination. Briefly, any perturbation on these detectors generates a nonlinear signal with higher amplitude than a dark current and lasts for hours. The traditional hypothesis used to explain this phenomenon is based on trapping/emission processes from deep-level defects in the space charge region (SCR) of the diode. Inspired by deep-level transient spectroscopy formalism, we have developed an analytical model describing the trap emission current from the SCR of the photodiode. We also take into account the intrinsic non-linearity of the source follower per detector ROIC architecture. Compared to data obtained on detectors built in-house at CEA-LETI, the model allows the estimation that a trap density on the order of the residual doping is enough to explain the persistence amplitude. A graded trap density in the SCR is in addition necessary to explain the persistence measurement as a function of the stress amplitude. Limits of the model are also underlined in the case of higher persistence amplitude. In this case, trap density should be close to the doping. This implies that *N* doping of the diode would be compensated, which is an extreme scenario out of the scope of this model.

Keywords Persistence · HgCdTe · SWIR detector · astronomy · modeling · extended defect

Introduction

For astronomy applications, the expected performance level of infrared (IR) detectors is extremely high. For the HgCdTe (MCT) industry, the quantum efficiency (> 80%), read-out noise (< $18e^-$), and dark current (< $0.01e^-/s$ at 100 K) is well controlled. However, one remaining characteristic limits the scientific use of these detectors: the persistence. In the short term, previous images leave their imprint and pollute the following images with time constants in the order of hours.

In the frame, the program ALFA[1] between ESA, the CEA-LETI, the CEA-IRFU, and the industrial company, Lynred, a large action is ongoing for setting up in Europe large-scale HgCdTe focal plane arrays for IR astronomy applications. For this development, an improvement in the persistence criteria would be a crucial advantage compared to existing detectors. However, the technological steps responsible for this degradation are not known, and the physical mechanisms involved are not well understood. In addition, there is no clear methodology to study this characteristic. In this context, this paper aims to develop an analytical model of persistence in order to provide a better understanding of the phenomenon, and to identify possible technological improvements for the next generation of ALFA detectors.

The model starts by considering the intrinsic non-linearity of the source follower per detector (SFD) ROIC architecture. This architecture is used on all read-out circuits of hybridized MCT detectors designed for low-flux astronomy applications. Then, the persistence model considers deep-level defects localized in the space charge region (SCR) of the diode. This explanation is based on the R. Smith model[2] that is widely accepted in the literature.[3] Our contribution is to consider the behavior of the traps in the specific case of the MCT material, and to develop the analytical formalism associated with it. The deep-level defect formalism largely inspired this work. To test the model, we compare it to actual data obtained

✉ T. Le Goff
titouan.legoff@cea.fr

[1] Univ. Grenoble Alpes, CEA - LETI, 17 Avenue des Martyrs, 38000 Grenoble, France

[2] Astrophysics Department-Orme Des Merisiers, CEA, IRFU, 91191 Gif-Sur-Yvette, France

on P/N, 2.1-μm cutoff wavelength, VGA format with the 15-μm pixel pitch detectors built in-house at CEA-LETI.

Integration Mode Non-Linearity

Before modeling the persistence signal, the intrinsic non-linearity of the SFD integration mode must be considered. With the SFD architecture, the photo-generated charges are directly integrated in the low diode capacitance of the pixel. Indeed, it allows a high conversion gain from accumulated charges to the measured output voltage. The read noise is consequently very low, lower than $18e^-$ on the LETI technology.[4] This architecture also allows non-destructive read-out over time. We refer to the term 'integration ramp' for this voltage sampling over time. The reset allows the evacuation of the accumulated charges to pass to the next acquisition.

However with a SFD pixel, we do not measure a current but instead a voltage change, due to a charge accumulation in a non-linear capacitance. The diode capacitance depends on the depletion size of the SRC W_{dep} according to Eq. 1, that shrinks as charges are accumulated, and that the voltage on the pixel drops as shown in Eq. 2:

$$C_{\text{diode}} = S_{\text{diode}} \frac{\epsilon}{W_{\text{dep}}} \tag{1}$$

$$W_{\text{dep}} = \sqrt{\frac{2\varepsilon}{qN_{\text{D}}}\left[V_{\text{bi}} - \left(V - V_{\text{app}}\right)\right]} \tag{2}$$

where S_{diode} is the surface of the diode, ϵ the dielectric permittivity of the MCT, N_{D} the doping, V_{bi} the built-in voltage, V_{app} the initial voltage applied with the reset, and V the floating voltage on the integration node. The doping of the abrupt P–N junction is supposed to be asymmetric with $N_A \gg N_{\text{D}}$. Consequently, the depletion region is expended only in the N-type absorbing layer.

In the test detectors of this study, there is no additional nodal capacitance and the parasitic capacitance of the ROIC is reduced by design. This parasitic capacitance adds to the diode capacitance and its value is 4 fF.[5,6] This is a main difference with ALFA detectors, on which there is an additional 20-fF fixed capacitance on the integration node.

The diode geometry of the 15 μm pitch pixel is not simple plane surface, the lateral sides must be considered.

Figure 1 shows a scheme of the cylindrical structure of the diode. Equation 3 expresses the SCR external surface expended in the N-type material. The upper side of the diode in the P region is not taken into account since the SRC does not extend to this region:

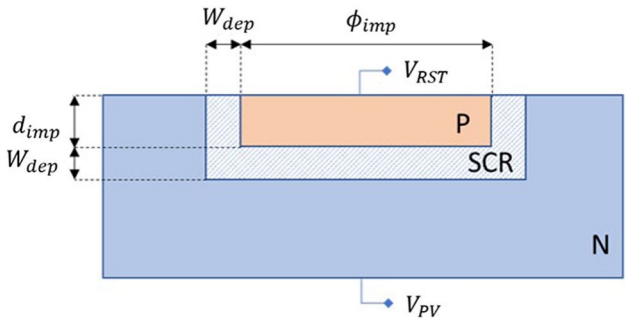

Fig. 1 Semi-cylindrical diode geometry of a pixel.

$$S_{\text{diode}} = \pi\left(W_{\text{dep}} + \frac{\Phi_{\text{imp}}}{2}\right)^2 + 2\pi\left(W_{\text{dep}} + \frac{\Phi_{\text{imp}}}{2}\right)\left(d_{\text{imp}} + W_{\text{dep}}\right) \tag{3}$$

The output voltage change of the pixel depends on its whole integration history.[7] From the definition of the differential capacitance of a diode, $C = \frac{\text{d}Q}{\text{d}V}$,[8,9] the expression of the voltage change on the diode due to the integration of a current over time is defined in Eq. 4:

$$\frac{dV}{dt} = \frac{I}{C} \tag{4}$$

with I in Eq. 5 being the current that depends on the dark current I_{dark} and the photonic current I_{Φ}:

$$I = I_{\text{dark}}\left(e^{\frac{q\left(V_{\text{app}}+V\right)}{\text{nkT}}} - 1\right) - I_{\Phi} \tag{5}$$

with n the ideality factor of the diode, k the Boltzman constant, and T the operating temperature.

To test the model, we illuminated a detector mounted in a cryostat with a black body surface at 50 °C through a very narrow field of view of F/21. The operating temperature was 100 K. The expected flux with these conditions is $562ph/s$/pix, corresponding to a current of $450e^-/s$/pix if the quantum efficiency is 80%. Figure 2 plots the integration ramp of a single pixel of the detector with red crosses. The best fit obtained with the model is plotted by the dark dashed line and this estimates a current of $455e^-/s$/pix and $n = 1.06$. The initial model parameters are ϕ_{imp}, d_{imp}, N_A, N_{D}, $T = 100K$, $I_{\text{dark}} = 10^{-2}e^-/s$, and $V_{\text{app}} = -400mV$. The only free parameters are the incident photonic current I_{Φ} and the diode ideality factor n. We also compare the result of the model with a simple linear regression of the ramp with the expected pixel capacitance at the initial bias $C = 17fF$. Plotted by the blue line, the regression estimates a current of $450e^-/s/pix$ and illustrates the non-linearity of the actual integration ramp.

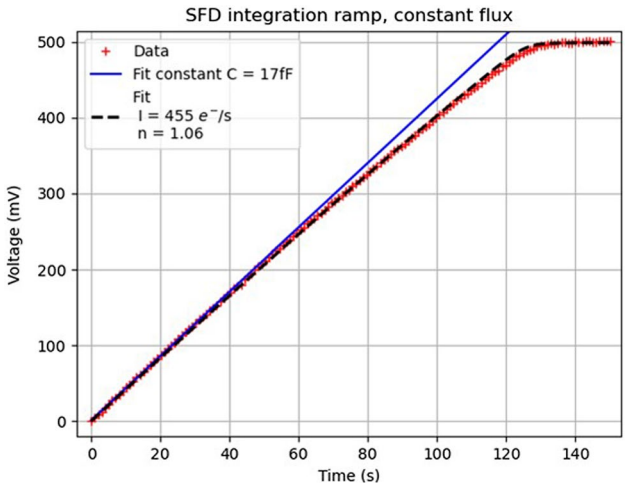

Fig. 2 Comparison of the integration ramp measured on a single pixel of a test detector by *red crosses* with the model in *black dotted line*. The *blue line* represents the integration of the same flux but in a constant capacitance of 17 Ff (Color figure online).

The criteria to validate the model were its ability to reproduce the non-linearity of the SFD integration ramp, not to estimate the incident flux with a high percentage of confidence. For this purpose, other methods such as polynomial fit are usually used.

With these parameters, the SCR shrinks by a factor of 30% and the pixel capacitance consequently changes by a factor of 20% during the integration.

Now that the non-linearity of the integrated signal due to the capacitance change is known, we can use the SFD model with a non-linear current corresponding to the persistence current. It will be possible to distinguish the contribution of the persistence current and the capacitance variation of the diode in the measured signal.

Persistence Signal Modeling

The first step of the model was to take into account the intrinsic non-linearity of the SFD pixel. Now, we can introduce the non-linear persistence current integrated in this non-linear capacitance.

The persistence model is based on trapping/emission processes of deep-level defects located in the SCR. During the integration, the SCR shrinks due to the accumulation of electrons in the diode capacitance. Defects that are now located in the neutral region of the *N*-type absorbing layer can capture an electron. Applying the reset to pass to the next image enlarges the SCR and occupied traps are now exposed to an electrical field. They consequently emit their electrons to reach their equilibrium state. This electron emission corresponds to the persistence signal. This explanation is based on the R. Smith model.[2] Let us now develop the associated analytical formalism. It is largely inspired by the deep-level transient spectroscopy (DLTS) formalism of Schröder [10].

A trap family is characterized by three parameters: its capture cross-section σ_n $[m^2]$, its energy in the band gap E_{T0} $[eV]$, and its density N_T $[m^{-3}]$. A hypothesis is that the emission cross-section of the traps is equal to their capture cross-section.[10] Its emission e_n $[s^{-1}]$ rate sums up all these properties, as expressed in Eq. 6:

$$e_n = \sigma_n v_{\text{th}} N_c \mathrm{e}^{-\frac{E_c - E_{T0}}{kT}} \tag{6}$$

with v_{th} the thermal velocity of electrons in the material and N_c the state density in the conduction band.

In the space charge region, the electron and hole capture is null. Considering traps whose energy level is higher than the mid-gap, the hole emission can be neglected. Defects are electrons traps in the *N*-type material. The occupied trap density variation in the SCR $\frac{\mathrm{d}n_T}{\mathrm{d}t}$ is inversely proportional to the electron density variation in the conduction band $\frac{\mathrm{d}n}{\mathrm{d}t}$ according to Eq. 7:

$$\frac{\mathrm{d}n_T}{\mathrm{d}t} = -\frac{\mathrm{d}n}{\mathrm{d}t} = -e_n n_T(t) \tag{7}$$

Up to now, we described the behavior of single point defect, which generates a single energy level in the band gap. However, the DLTS technique applied on MCT can rarely unambiguously attribute an energy and capture cross-section to traps. Indeed, DLT spectra are usually quite broad and the energy associated with the trap would be higher than the band gap.[11] Moreover, even if the signature of a single trap in a N/P short wave infrared (SWIR) photodiode could be estimated,[11] the time constants used in DLTS is completely different when with persistence. Persistence time constants are indeed on the order of several hours, whereas DLTS scans a much faster trap response.

To explain the broad DLT spectra, either the capture cross-section of the traps depends on temperature,[12] or this is the signature of spatially extended defects such as dislocation.[13,14] The silicon literature can also provide some perspective. The dominant theory to interpret these large spectra is to consider that an extended defect such as dislocation will generate an energy distribution in the band gap.[15,16] Moreover, the MCT is a ternary semiconductor alloy. In an alloy, even a single point defect generates energy distribution, due to the introduced disorder and material composition fluctuation. Omling et al.[17,18] show that a Gaussian distribution can explain the symmetric broadening of DLT spectra measured in semiconductor alloys.

Instead of the commonly used sum of exponential to fit the persistence signal[19–21] our model is based on this energy distribution. The capture cross-section of this trap distribution

is probably also affected, but our model first focuses on the energy distribution.

To model the response of extended defects, the literature suggests the introduction of a disorder term, expressed as a ponderation Gaussian function. Equation 8 describes the occupied trap density evolution with time:

$$n_T(t) = n_T(0) \int_0^\infty g(E) e^{-e_n(E)t} \mathrm{d}E \tag{8}$$

with $n_T(0)$ the initial occupied trap density and $g(E)$ the ponderation function, centered around the central energy level of the distribution E_{T0} and with a broadening σ_T:

$$g(E) = \frac{1}{\sigma_T \sqrt{2\pi}} e^{-\frac{(E_{T0}-E)^2}{2\sigma_T^2}} \tag{9}$$

Then, each energy level of the distribution now emits its electrons according to its own emission rate, as shown in Eq. 10:

$$e_n(E) = \sigma_n v_{th} N_c exp\left[-\frac{E_c - E}{kT}\right] \tag{10}$$

When emitting their electrons, the trap distribution generates a current. The development below is adapted from Ref. 10 .

The emission current is related to the total amount of charges emitted by traps as shown in Eq. 11:

$$I_e(t) = qS \int_{W_0}^{W} \frac{\mathrm{d}n}{\mathrm{d}t} dx = qSe_n n_T(t)\left[W - W_0\right] \tag{11}$$

with S the diode surface, W_0 the initial SCR size, and W the SCR size variation with time. W_0 is not neglected since only small biases are applied on our detector, − 900 mV at maximum.

The displacement current described in Eq. 12 is also present due to the charge density in the SCR variation during the process. Indeed, traps occupied by electrons have an opposite charge sign than the initial doping N_D. Consequently, the electrical field in the SCR also changes due to this charge compensation:

$$I_d(t) = qS \int_{W0}^{W} \frac{\mathrm{d}b_T}{\mathrm{d}t} \frac{x}{W} \mathrm{d}x = -qSe_n n_T \left[\frac{W^2 - W_0^2}{2W}\right] \tag{12}$$

Neglecting the dark current of the diode, the total current in Eq. 13 is equal to the sum of the emission current and the displacement current:

$$I_{\mathrm{tot}} = I_e + I_d = qS\left[W - W_0 - \frac{W^2 - W_0^2}{2W}\right] e_n n_T \tag{13}$$

Next, this current is integrated in the non-linear capacitance of the SFD pixel. Its capacitance always changes due to the voltage variation in the pixel, but now also due to the charge density compensation in the SCR. Equation 14 demonstrates that the SCR size depends on the ratio of the occupied trap density and the initial doping:

$$W = \sqrt{\frac{2\varepsilon\left[V_{bi} - \left(V_{stress} + V\right)\right]}{qN_D}} \sqrt{\frac{1}{1 - \frac{n_T}{N_D}}} \tag{14}$$

For a trap density on the order of 10% of the initial doping, the corresponding capacitance variation is 2%. However, for a higher trap density, the capacitance variation contribution to the persistence signal becomes less and less negligible.

A result of the model is presented on Fig. 3. For this simulation, the parameters are $V_{\mathrm{stress}} = -900mV$, $\sigma_n = 10^{-17}cm^{-2}$, $n_T = 10^{14}cm^{-3}$, and $E_{T0} = 0.32eV$. The black crosses represent the simulation for a single energy level in the band gap. It has a simple exponential behavior. When introducing the energy broadening, persistence now has a faster dynamic at the beginning of the integration and a slower one at the end, compared to the exponential dynamic.

This broadening does not impact on the persistence amplitude. Only the trap density and its ratio with the initial doping changes the persistence amplitude. However if the broadening is too large, the persistence signal does not reach the amplitude asymptote. The persistence amplitude seems to be low, but only because the integration time is too short compared to the persistence time constant.

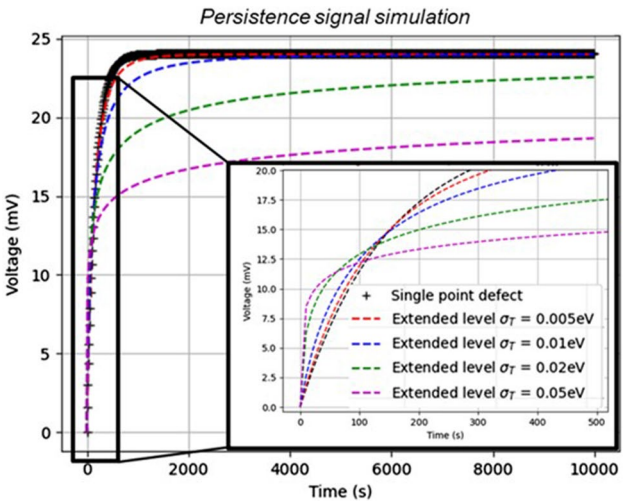

Fig. 3 Persistence signal simulation for several energy distribution broadening *σ_T*. The *framed inset at the lower right* shows a zoom of the first seconds of the integration ramp.

Comparison with Persistence Measurements and Limits

To compare the model, we measure persistence with the electrical stress procedure.[22] It simply consists in changing the applied voltage on the diode through two resets at two different reset voltages. It has for its main impact to enlarge the SCR if the first reset polarizes the diode at 0 V and the second polarizes the diode in reverse. This protocol is similar to applying a reset after the integration of a flux, but it has the advantage of being sure that all the traps are filled before the measurement. It also enables the probing of a specific volume of the diode as a function of the applied voltage.[23]

Figure 4 shows that the model can reproduce with a very low residual the non-linear shape of the persistence signal. The detector under test is referred to as a second-generation technology detector. The fixed fitting parameters are $V_{\text{stress}} = -900mV$ and $\sigma_n = 10^{-17}cm^{-2}$. The output parameters are $n_T = 1.310^{14}cm^{-3}$, $E_{T0} = 0.396eV$ and $\sigma_T = 20meV$. The gap of the absorbing material is $E_g = 0.59eV$. The energy broadening is consequently only 3% of the band gap.

The persistence amplitude is $23mV$, and the model can estimates the necessary trap density to explain this amplitude, $n_T = 1.310^{14}cm^{-3}$. It is on the order of the residual doping, which is the uncontrolled doping due to all the residual impurities in the material.

However, the estimation of the central energy of the distribution depends on the input capture cross-section. All we can say is that the couple (σ_n, E_{T0}) must satisfy the emission rate $\frac{1}{e_n} = 900 \pm 50s$. Measurements of persistence as a function of temperature are required to estimate both the capture cross-section and the central energy of the distribution. The choice of the capture cross-section and central energy of the distribution have no impact on the distribution broadening σ_T. Moreover, the capture cross-section of the trap distribution is probably not a single value; it should also be a capture cross-section distribution. This consideration is important to improve the accuracy of the model, but would not change our conclusions. A trap energy distribution can reproduce the non-linear shape of the persistence signal.

With the fitting parameters obtained on data at the stress amplitude of 900 mV, it is possible to run the model with the estimated trap density and energy level at other stress amplitudes. To compare these estimations, we have also characterized persistence on the same detector as a function of the stress amplitude. Figure 5 plots the persistence amplitude estimated by the model with trap density $n_{T0} = 1.310^{14}cm^{-3}$, and the measured persistence amplitude as a function of the stress amplitude. When the stress amplitude decreases, the expected persistence amplitude is lower than the measured persistence amplitude. Moreover, the evolution of the persistence amplitude with the stress amplitude is not linear, and is different between the measurement and the model.

One solution to explain the differences between the data and the model is to consider a graded trap density in the SCR. The mean trap density necessary to reproduce the measured persistence amplitude with the model is represented by blue crosses on the figure. In the frame of the model, the trap density should be two times higher for

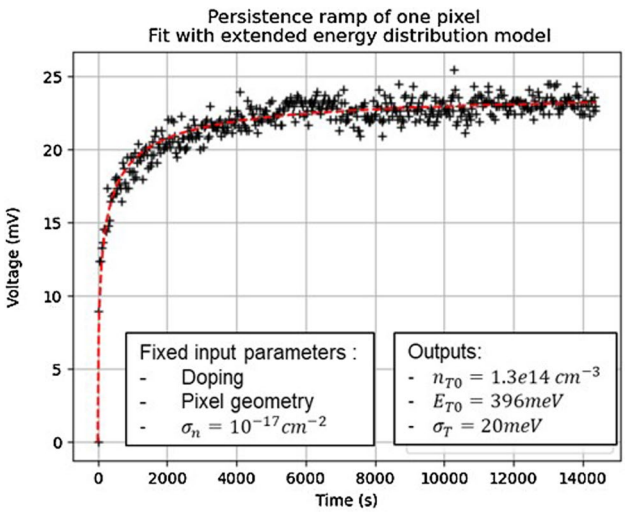

Fig. 4 Comparison of a persistence integration ramp (*dark crosses*) and the best fit obtained with the model (*dotted red line*). The persistence ramp comes from a single pixel of the second-generation technology detector. The stress amplitude is − 900 mV performed at the temperature of 100 K (Color figure online).

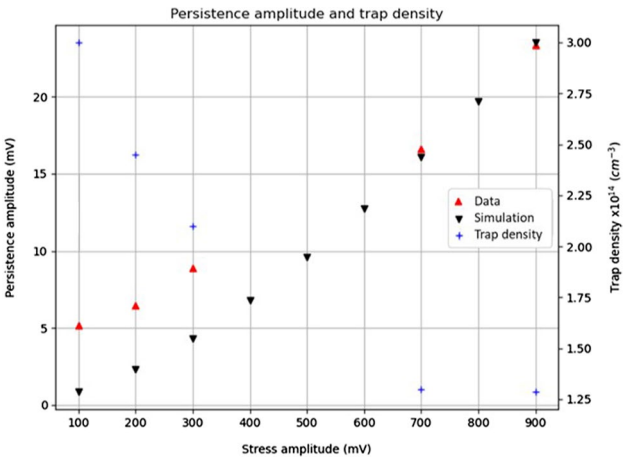

Fig. 5 Comparison of measured and simulated persistence amplitude as a function of the stress amplitude. The trap density and energy level obtained with the fitting at 900 mV are used to run the model at other stress amplitudes. The persistence amplitude estimated by the model is plotted with *black triangles*. The necessary trap density to explain the measurements is indicated on the *right-hand scale* and by *blue crosses* (Color figure online).

the simulation at the stress amplitude of 100 mV than at 900 mV.

This gradient of trap density could be explained by surface traps or larger trap densities close to the junction of the diode. For lower stress amplitudes, their contribution would take a larger part in the persistence signal, whereas for higher stress amplitudes a larger SCR volume with a lower trap density has been probed.

The limits of the model are also investigated in the case of detectors with higher persistence amplitudes. Indeed, in our first-generation technology detector, the persistence amplitude was ten times higher than in the second-generation ones. Figure 6 illustrates the persistence ramp of one pixel of the first-generation detectors and the best fit of the model. The initial parameters are similar to the ones used for Fig. 4 except for the temperature $T = 120$K. We showed in a previous paper that the persistence amplitude does not depend on the temperature in this detector.[22]

The model can still interpolate the persistence ramp with low residuals. The central energy of the distribution for both detectors is very similar.

The necessary trap density to explain this high persistence amplitude is also very different from this first-generation detector. The trap density should be so high compared to the initial doping that the semiconductor would be in a compensated regime. The physics of this regime are completely out of the scope of our model. We also tried to consider deep-level defects located in the *P* region of the diode. Even if the trap density decreases with this consideration, the conclusion is still the same. The trap density is very high compared to the initial doping. Consequently, a model based only on deep-level defects located in the SCR is incomplete as an explanation of the high persistence amplitude. Technological steps or other types of defects must be responsible of this high persistence amplitude.

Discussion

Considering the persistence models, including the present one, published in the literature, the initial hypothesis is that the persistence comes from trapping/emission processes due to defects located in the space charge region of the diode. However, the nature of the defects is different.

The persistence dynamic is faster than an exponential at the beginning of the integration and slower at the end of the measurement. A model with at least three exponentials is necessary to obtain a fitting quality similar to the one obtained with the model described in this paper. In fact, persistence ramps are often fitted with a model based on a sum of exponentials in the literature,[20] illustrated in Fig. 7. The interpretation is that each time constant associated with an exponential is representative of a trap family. These traps would generate discrete energy levels in the band gap. However, estimated time constants differ by an order of magnitude. This issue can be related to numerical issues more than to physical ones. Indeed, no deep-level defect characterization applied on MCT gives capture cross-sections and energy levels associated with the time constants estimated with multi-exponential fitting. Moreover, adding another exponential term to the fit shifts the previous time constants, leading to different equivalent activation energies for the traps.

The model presented in this work is also based on emission processes of defects located on the SCR, but is conversely based on a single trap family that generates a broad

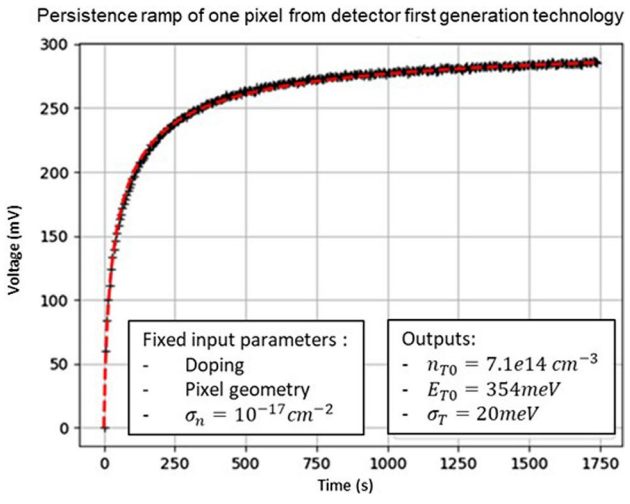

Fig. 6 Model applied to estimate the trap density in the first-generation technology detector. The stress amplitude is − 900 mV performed at the temperature of 120 K.

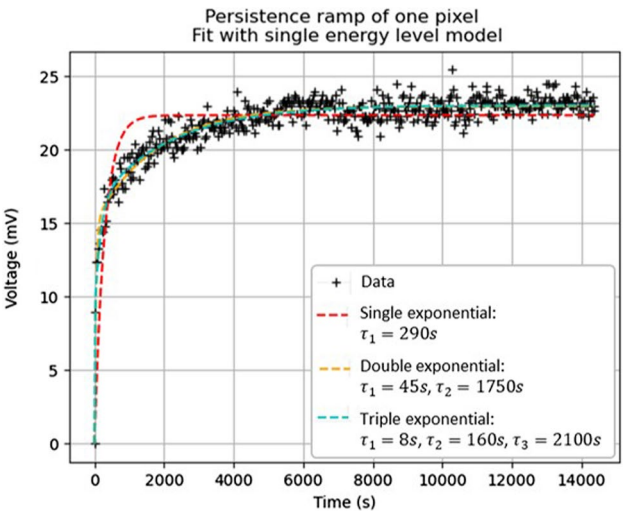

Fig. 7 Persistence measurement ramp compared with best fit obtained with models including one, two, or three exponentials.

energy distribution in the band gap. The theoretical behavior of traps in semiconductor alloys, spatially extended defects, and DLTS measurements on MCT found in the literature support this hypothesis.

On the other hand, the European Southern Observatory (ESO) detector group choose to fit the persistence ramp with a multi-exponential model, but whose time constants are fixed.[24] Repeating the measurement at several temperatures, the trap density distribution in the time constant bins change, building the so-called 'waterfall diagram'. They attribute the peak trap density time constant change with temperature to the presence of a single trap family. The trap family with a broad energy distribution developed in this model could be in agreement with the interpretation of the ESO team.

Conclusions

We have developed an analytical model based on semiconductor physics to explain the phenomenon of persistence. This model is based on trapping/emission processes from a deep level located in the SCR of the pixel. Considering the special case of HgCdTe, these defects are more likely to generate an energy distribution in the band gap instead of a single level. The literature of defect characterization of HgCdTe and semiconductor alloy physics supports this hypothesis. When emitting their electrons, traps generate a current that is related to the total amount of charges and the charge density variation in the SCR. Occupied traps have an opposite charge sign to that of initial doping, thus compensating the charge density in the SCR. This current is then integrated in the non-linear capacitance of the diode due to the specific integration strategy of the SFD architecture. The capacitance is non-linear due to the applied voltage variation on the diode and to the charge compensation of the SCR. To sum up, the persistence signal is the result of the integration of a non-linear current in a non-linear capacitance. The model requires the geometrical and doping parameters of the diode as fixed input values.

This model is then compared to persistence measurements performed on two detectors, from first- and second-generation technology. The model reproduces very well the non-linearity of the persistence signal. The required energy broadening is on the order of 3% of the band gap. The capture cross-section and the central energy of the distribution could not be estimated. Measurements at several temperatures are required to estimate these two parameters. Their estimation would provide valuable information for operating a detector. Indeed, the optimal temperature for which the persistence time constant is very long compared to the integration time used in astronomy could be estimated.

For the second-generation detector, a trap density on the order of the residual doping is sufficient to explain the low persistence amplitude. Then, a graded trap density in the SCR with a higher trap density close to the junction is one explanation to reproduce the measured persistence amplitude as a function of the stress amplitude.

However, the higher persistence amplitude measured on our first-generation detector is not explained by the model. The conclusion is that, on this detector, persistence comes from another type of defect in the pixel. For instance, we are working on how to take into account traps located at the interface between the absorbing layer and the passivation. This interface is indeed known to have large trap densities. The interesting point is that the large difference between the two technologies is only revealed by persistence characterization. This remark indicates the relevance of persistence characterization in a detector process line to probe the influence of technological steps that cannot be investigated by classical characterization techniques. However, a study on a larger number of samples is necessary to study the link between persistence and passivation-related defects.

The model describes the emission phase of the persistence with the hypothesis that all the traps are filled before the stimulation. Another improvement would be to consider the capture phase of the electrons by the traps during an illumination. The procedure to characterize the capture rate of persistence could be similar to the electrical stress used in this work. The bias applied during the equilibrium phase should be a reverse bias, ensuring that all the traps in the SCR are empty, and that the stress would be to reverse bias the detector at a lower level.

Acknowledgments The authors would like to thank the Labex FOCUS (ANR-11-LABX-0013), the European Space Agency (ESA) and the European Commission in the frame of H2020 ASTEROID development program strategy for funding the detectors used in this work.

Conflict of interest The authors declare that they have no conflict of interest.

References

1. B. Fièque, A. Lamoure, F. Salvetti, S. Aufranc, O. Gravrand, G. Badano, O. Boulade, S. Mouzali, S. Basa, Development of Astronomy Large Focal Plane Array "ALFA" at Sofradir and CEA, in *High Energy, Optical, and Infrared Detectors for Astronomy VIII*, vol. 10709(SPIE, Washington, 2018).
2. R. M. Smith, M. Zavodny, G. Rahmer, et M. Bonati, A Theory for Image Persistence in HgCdTe Photodiodes, in *Proceedings of SPIE* vol. 7021 (2008).
3. S. Tulloch, and E. George, Predictive Model of Persistence in H2RG Detectors. *J. Astron. Telesc. Instrum. Syst.* 5, 036004 (2019).
4. B. Fieque, L. Martineau, E. Sanson, P. Chorier, O. Boulade, V. Moreau, H. Geoffray, Infrared ROIC for Very Low Flux and Very Low Noise Applications. in *Proceedings of SPIE*, vol. 8176 (2011).

5. O. Boulade, N. Baier, P. Castelein, C. Cervera, P. Chorier, G. Destefanis, B. Fièque, O. Gravrand, F. Guellec, V. Moreau, P. Mulet, F. Pinsard, J.-P. Zanatta, Development and Characterisation of MCT Detectors for Space Astrophysics at CEA. in *Proceedings of SPIE*, vol. 10563 (2017).
6. C. Cervera, O. Boulade, O. Gravrand, C. Lobre, F. Guellec, E. Sanson, P. Ballet, J.L. Santailler, V. Moreau, J.P. Zanatta, B. Fieque, and P. Castelein, Ultra-Low Dark Current HgCdTe Detector in SWIR for Space Applications. *J. Electron. Mater.* 46, 6142–6149 (2017).
7. N. Bezawada, D. Ives, et D. Atkinson, Conversion Gain Non-Linearity and Its Correction in Hybridised Near Infrared Detectors. in *Proceedings of SPIE*, vol 6690, (2007).
8. U. Jadli, F. Mohd-Yasin, H.A. Moghadam, J.R. Nicholls, P. Pande, and S. Dimitrijev, The Correct Equation for the Current Through Voltage-Dependent Capacitors. *IEEE Access* 8, 98038–98043 (2020).
9. G.P. Weckler, Operation of p-n Junction Photodetectors in a Photon Flux Integrating Mode. *IEEE J. Solid-State Circuits* 2, 65–73 (1967).
10. D. K. Schroder, Semiconductor Material and Device Characterization: Third Edition. (Wiley-IEEE press, 2005)
11. L. Rubaldo, A. Brunner, J. Berthoz, N. Péré-Laperne, A. Kerlain, P. Abraham, D. Bauza, G. Reimbold, and O. Gravrand, Defects Study in Hg x Cd1-x Te Infrared Photodetectors by Deep Level Transient Spectroscopy. *J. Electron. Mater.* 43, 3065–3069 (2014).
12. C.A. Merilainen, and C.E. Jones, Deep Centers in Gold-Doped HgCdTe. *J. Vac. Sci. Technol. A Vac. Surf. Films* 1, 1637–1640 (1983).
13. J. F. Barbot, Deep Level Transient Spectroscopy Measurements in Hg0.3Cd0.7Te Single Crystals, Phys. Status Solidi (a), **124**, 2, 513–517, (1991).
14. D. Johnstone, T.D. Golding, R. Hellmer, J.H. Dinan, and M. Carmody, Characterization of HgCdTe Diodes on Si Substrates using Temperature-Dependent Current-Voltage Measurements and Deep Level Transient Spectroscopy. *J. Electron. Mater.* 36, 832–836 (2007).
15. W. Schröter, J. Kronewitz, U. Gnauert, F. Riedel, and M. Seibt, Bandlike and Localized States at Extended Defects in Silicon. *Phys. Rev. B* 52, 13726 (1995).
16. T. Figielski, Electron Emission from Extended Defects: DLTS Signal in Case of Dislocation Traps, Phys. Status Solidi (a), **121**, 1, 187–193, (1990).
17. P. Omling, E. R. Weber, L. Montelius, H. Alexander, et J. Michel, Electrical Properties of Dislocations and Point Defects in Plastically Deformed Silicon, *Physical Review B*, vol. 32, n° 10, p. 6571-6581, (1985)
18. P. Omling, E.R. Weber, L. Montelius, H. Alexander, and J. Michel, Electrical Properties of Dislocations and Point Defects in Plastically Deformed Silicon. *Phys. Rev. B* 32, 6571 (1985).
19. R. M. Smith, M. Zavodny, G. Rahmer, et M. Bonati, Calibration of Image Persistence in HgCdTe Photodiodes, *in Proceedings of SPIE*, vol 7021, (2008).
20. Y. Zhou, D. Apai, B.W. Lew, and G. Schneider, A Physical Model-Based Correction for Charge Traps in the Hubble Space Telescope's Wide Field Camera 3 Near-IR Detector and its Applications to Transiting Exoplanets and Brown Dwarfs. *Astron. J.* 153, 243 (2017).
21. S. Tulloch, Persistence Characterisation of Teledyne H2RG Detectors. (Scientific Detector Workshop 2017), Baltimore, *arXiv e-prints*, arXiv:1807.05217v1 [astro-ph.IM], (2018).
22. T. Le Goff, N. Baier, O. Gravrand, O. Boulade, et T. Pichon, Persistence and Dark Current Characterization on HgCdTe Short Wave Infrared Imagers for Astronomy at CEA and Lynred. in *Proceedings of SPIE*, vol. 11454 (2020).
23. R. E. Anderson, M. Regan, J. Valenti, et E. Bergeron, Understanding Persistence: A 3D Trap Map of an H2RG Imaging Sensor, *arXiv e-prints*, vol. 1402, p. arXiv:1402.4181, (2014).
24. D. Ives, D. Alvarez, N. Bezawada, E. George, et B. Serra, Characterisation, Performance and Operational Aspects of the H4RG-15 Near Infrared Detectors for the MOONS Instrument, in *Proceedings of SPIE*, vol. 11454 (2020)